Petroleum Science 22 (2025) 5268–5276

Contents lists available at ScienceDirect

Petroleum Science

journal homepage: www.keaipublishing.com/en/journals/petroleum-science

Grain boundary strength in methane hydrates

Ke Xu [a,b], Rui Ma [c], Yong-Xiao Qu [a], Zhi-Sen Zhang [a], Jian-Bin Xu [b,*], Jian-Yang Wu [a,c,**]

[a] Department of Physics, Research Institute for Biometrics and Soft Matter, Jiujiang Research Institute and Fujian Provincial Key Laboratory for Soft Functional Materials Research, Xiamen University, Xiamen, 361005, Fujian, China
[b] Department of Electronic Engineering and Materials Science and Technology Research Center, The Chinese University of Hong Kong, Shatin, N.T., Hong Kong SAR, 999077, China
[c] NTNU Nanomechanical Lab, Norwegian University of Science and Technology (NTNU), Trondheim, 7491, Norway

ARTICLE INFO

Article history:
Received 2 January 2025
Received in revised form
16 March 2025
Accepted 18 October 2025
Available online 27 October 2025

Edited by Teng Zhu

Keywords:
Methane hydrate
Grain boundary
Mechanical properties
Molecular dynamic
Machine learning

ABSTRACT

Grain boundaries (GBs) in natural gas hydrates (NGHs) are ubiquitous crystal imperfection that undermine the stability of NGHs. In this study, we report the diverse cage structures and mechanical properties of GBs in methane hydrates using molecular dynamic (MD) simulations with advanced machine learning (ML) techniques. Employing a Random Forest-based feature extraction method, we weight and rank the 84 degrees of freedom to eliminate cage types with zero weight. Notably, 11 cage types identified through principal component analysis (PCA) play critical roles in dictating the overall mechanical properties of GBs in methane hydrates. This work establishes an MD-ML framework to elucidate the relationships between GB composition-structure-mechanical properties in NGHs, which is of great importance in predicting the mechanical stability of sediment-hosted NGHs.

1. Introduction

Clathrate hydrates (CHs) consist of water molecules hydrogen-bonded (HB) to form cage structures that trap small molecules as guests under harsh conditions of high-pressures and low temperatures (Sloan, 2003; Hester and Brewer, 2009). Depending on the size and shape of guest molecules, three types of clathrate hydrate structures including cubic structure I (sI), cubic structure II (sII), and hexagonal structure H (sH) can mainly form in natural settings. The most important clathrate hydrate is natural gas hydrates (NGHs) that massively occurred in permafrost and marine sediments. NGHs are considered potential future energy resource, with total resource value of 41.46×10^{12} m^3 at the year of 2050, which is about 10% of total natural gas resource in conventional reservoir (Pang et al., 2021). NGHs are garnering increasing attention due to their numerous advantages, including wide distribution, large reserves, and low pollution (Zi et al., 2018; Lu et al., 2020; Wei et al., 2024).

NGHs-bearing sediments show enhanced geo-mechanical properties compared to the native sediments because sediment frameworks are critically cemented by NGHs. When suffering natural and anthropogenic disturbances such as submarine (Zhang et al., 2021a), coastal development (Liu et al., 2019), and petro-activities (Boswell, 2009), NGHs could experience large deformations, causing stress-induced dissociation into the fluid phase of water and methane gas (Freij-Ayoub et al., 2007; Zhang and Taboada-Serrano, 2020; Liu et al., 2022a). Such hydrate dissociation significantly reduces the sediment strength and stiffness, thereby resulting in geo-mechanical instabilities. It is therefore suggested that the mechanical characteristics of NGHs themselves have profound implications in the seabed stability (Ning et al., 2012), the safety of ocean engineering (Kvenvolden, 1999), the natural gas recovery and CO_2 sequestration by CH_4–CO_2 replacement (Zhang et al., 2022), as well as hydrate-based CO_2 geological storage (Ota et al., 2005; Tung et al., 2011). Given the importance of NGH mechanical properties, extensive efforts have been devoted over recent years to a deep understanding of mechanical behaviors of NGHs and other gas hydrates, mainly focusing on internal influencing factors such as guest occupancy (Yu et al., 2019), water vacancy (Peters et al., 2008), guest size (Vlasic

* Corresponding author.
** Corresponding author.
E-mail addresses: jbxu@ee.cuhk.edu.hk (J.-B. Xu), jianyang@xmu.edu.cn (J.-Y. Wu).
Peer review under the responsibility of China University of Petroleum (Beijing).

https://doi.org/10.1016/j.petsci.2025.10.018

et al., 2017), grain size (Qin et al., 2021), and so forth (Li et al., 2016). It was found that flawless monocrystalline gas hydrates (MCGHs) yielded Young's modulus and failure strength up to GPa-level, as well as mechanically fail with brittle fractures.

In contrast, polycrystalline methane hydrates (PCMHs) exhibited maximum strength up to hundred-MPa level (Stern et al., 1996, 1998; Durham et al., 2003a, 2003b; Wu et al., 2015; Cao et al., 2021; Sveinsson et al., 2021), with several times lower than MCGHs. Moreover, PCMHs demonstrated exceptional long-range ductile flow characteristics, where X-ray analyses revealed that PCMHs undergoes a process of solid-state disproportionation or exsolution during deformation (Stern et al., 1996, 1998). Molecular dynamics (MD) simulations suggested that the combination of structural transformations and grain-boundary (GB) sliding are the main sources of the long-range plastic flow stress (Wu et al., 2015; Sveinsson et al., 2021). More intriguingly, there existed crossover in the mechanical strength of PCMHs at critical grain size, below which, grain size-strengthening behavior is identified, whereas above which, it is observed grain size-weakening behavior (Wu et al., 2015; Sveinsson et al., 2021). The grain boundary (GB) networks that surround crystalline hydrate grains (Murshed et al., 2008) play pivotal roles in the anomalous mechanical behaviors of PCMHs, as well as the prevailing failure mode (Zhang et al., 2021b).

In polycrystalline NGHs, however, GB networks are complex molecular structures (Wu et al., 2015), which are mainly structurally characterized by amorphous NGHs with diverse cages, amorphous water, and methane gas (Max et al., 2006). In addition, GBs are multiple metastable structures compared to the native crystalline hydrates, and they are liable to undergo structural transformations in response to depressurizing, chemical, mechanical or thermal stimuli. Such mutable GBs play an important role in modifying the microstructures of PCMHs, which complicates the stability and mechanical properties of PCMHs. Due to the limitations of nanoscale visualization for NGHs, however, it still remains challenge to experimentally examine the molecular basis of GBs and their effects on the mechanical properties of NGHs (Cao et al., 2021).

Herein, we report an in-depth analysis of GB structures and their mechanical properties in methane hydrates by molecular dynamics (MD) simulations combined with advanced machine learning (ML) techniques. The GB composition mainly consists of two parts. One part is the overall properties of the interface structure, including grain boundary energy, GB angles and mechanical properties, etc., which is described in Supplementary Material S1. The other part is local structural information. We streamline 84 degrees of freedom using a Random Forest-based feature extraction method and employ deep neural network (DNN) to well-predict the mechanical properties of GBs across an extensive set of low to high misorientation angle (θ) in methane hydrates. Our as-developed MD-ML framework not only enhances the predictive accuracy of GB mechanical properties in methane hydrates but also uncover the mechanisms by which specific alterations in GB-related cage structures influence the mechanical behaviors of methane hydrate. This work provides the relationships of microstructure-mechanical properties in NGHs, as well as underscores the critical roles of GB microstructures in governing the mechanical stability of sediment-hosted NGHs.

2. Models and methods

2.1. Workflow

Fig. 1 shows the workflow of this study for GB structures and GB mechanical properties in methane hydrate using a combination of MD and ML methods. NGHs are hosted by sediments (Fig. 1(a)), in which NGHs are polycrystalline structures, containing GBs. In this study, a number of 1250 models of symmetrical GB structures of sI methane hydrate are constructed using straightforward method based on the coincidence site lattice (CSL) model. As-constructed GBs with misorientation angle (θ) varying from around 5.2°–45°, in which the definition of θ and more typical GBs with different θ are described in Supplementary Material S1.1 and Fig. S1. As a result of wide range of θ, GBs show diverse cage configurations (Fig. 1(d) and (e)). Structural information of GBs is quantitatively characterized by GB length (L_{GB}) and GB energy (γ) (Supplementary Material S1.2). The clathrate cages are identified using the hierarchical topology of rings (HTR) algorithm (Liu et al., 2022b) (Supplementary Material S1.3 and Fig. S2). It is identified a total of 80 species in clathrate cages, including conventional cages of 5^{12} and $5^{12}6^2$ in sI hydrate, as well as amorphous water (W_A). Stretching MD simulations are conducted until the separation of GBs, and three mechanical properties, namely, Young's modulus E, tensile strength σ^m (the peak stress value in the stress-strain curves), and ultimate strain ε^b (the critical strain at which the uniaxial stretch stress occurs) are collected as mechanical features of GBs in methane hydrates containing approximately 5000–30,000 molecules depending on θ. Note that E of methane hydrates is obtained by linear fitting of the uniaxial tensile stress-strain curves with strain range of 0–1%. More detailed information of MD simulations refers to Supplementary Material S2. Those microstructural information and mechanical properties of GBs are the datasets for ML study (Fig. 1(f)–(i)).

2.2. Random Forest optimization descriptor selector

In this work, Random Forest (RF) is adopted to optimize the descriptor selector in predicting the mechanical properties of GBs in methane hydrates. RF is a bagging method in ensemble algorithms, which combines multiple decision trees. Within RF, a multitude of decision trees during the training is constructed, and then the class (mode of the classes) for classification or the mean prediction for regression from the individual trees is output. As-constructed decision trees differ from each other, improving the diversity of as-investigated system and enhancing the performance of classification. RF can produce high-dimensional data without requiring a reduction of dimensionality or feature selection. In addition, RF assesses feature importance by evaluating how much the tree nodes using a particular feature reduce impurity across all trees in the forest.

2.3. DNN model selection and performance

Based on MD simulations and RF optimization descriptor selector, phase-dependent relationships between microstructural information and mechanical properties of 1250 GBs are established. Such relationships are integrated into our as-developed DNN model for identification. The descriptors are utilized for training, validating and testing our as-developed DNN model. Using our well-developed DNN model, the mechanical properties of GBs are predicted with 84 degrees of freedom of microstructural information including 80 cage-type structures, W_A, G_L, γ, and θ. Note that the cage information and W_A are local properties, while G_L, γ, and θ are global information.

3. Results and discussion

3.1. Microstructures in GBs of methane hydrates

Fig. 2(a) presents zoomed-in snapshots of 8 GB-contained bicrystalline methane hydrates with ① $\varepsilon^b{}_{min}$ and ② $\varepsilon^b{}_{max}$, ③ $\sigma^m{}_{min}$ and ④ $\sigma^m{}_{max}$, ⑤ θ_{min} and ⑥ θ_{max}, ⑦ γ_{min} and γ_{max}. As is indicated, bicrystalline methane hydrates with different properties show

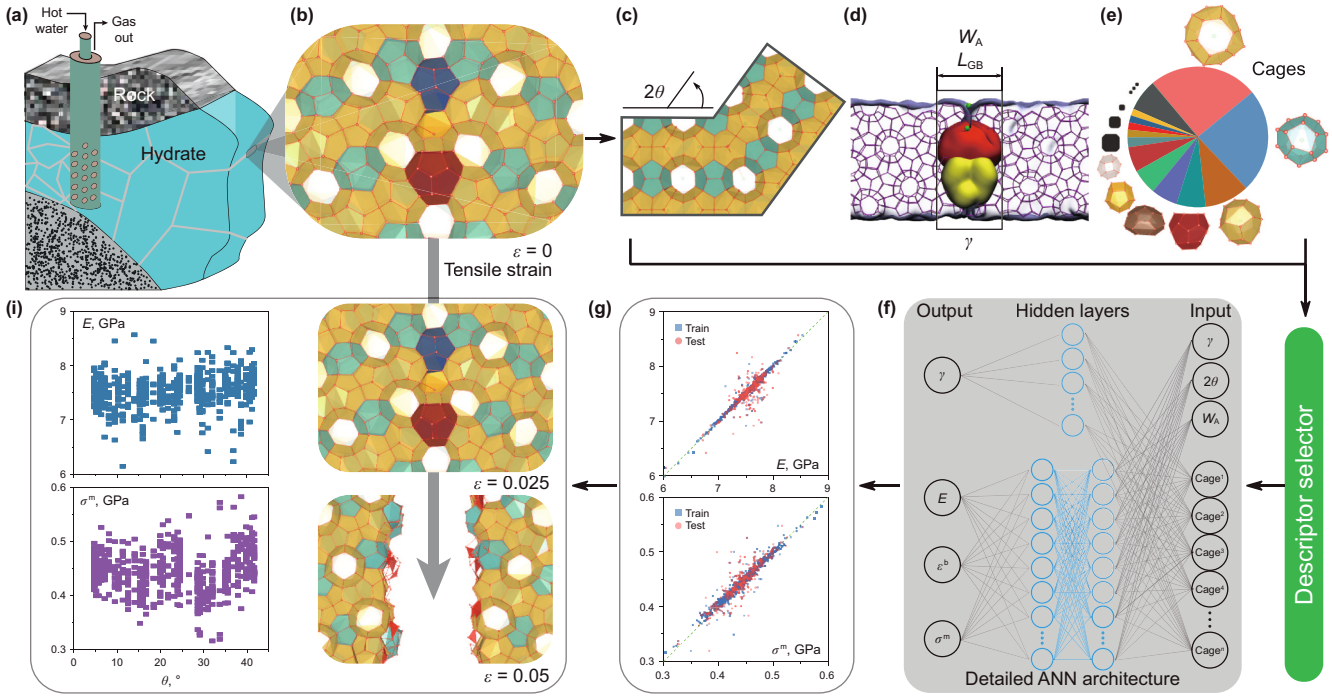

Fig. 1. Workflow for predicting the mechanical properties of GB structures in methane hydrates. (**a**) and (**b**) Schematics of sediment-hosted natural gas hydrates and GBs of methane hydrates. (**c**) A typical symmetrical GB structure with misorientation angle θ in methane hydrate. (**d**) Structural information of GBs such as GB length and energy are obtained from MD simulations. (**e**) Clathrate cages in GBs are identified by the hierarchical topology ring (HTR) algorithm (Liu et al., 2022b). (**f**)–(**i**) All GB information is passed as an input layer to an artificial neural network (ANN) and trained with mechanical properties as prediction targets for prediction.

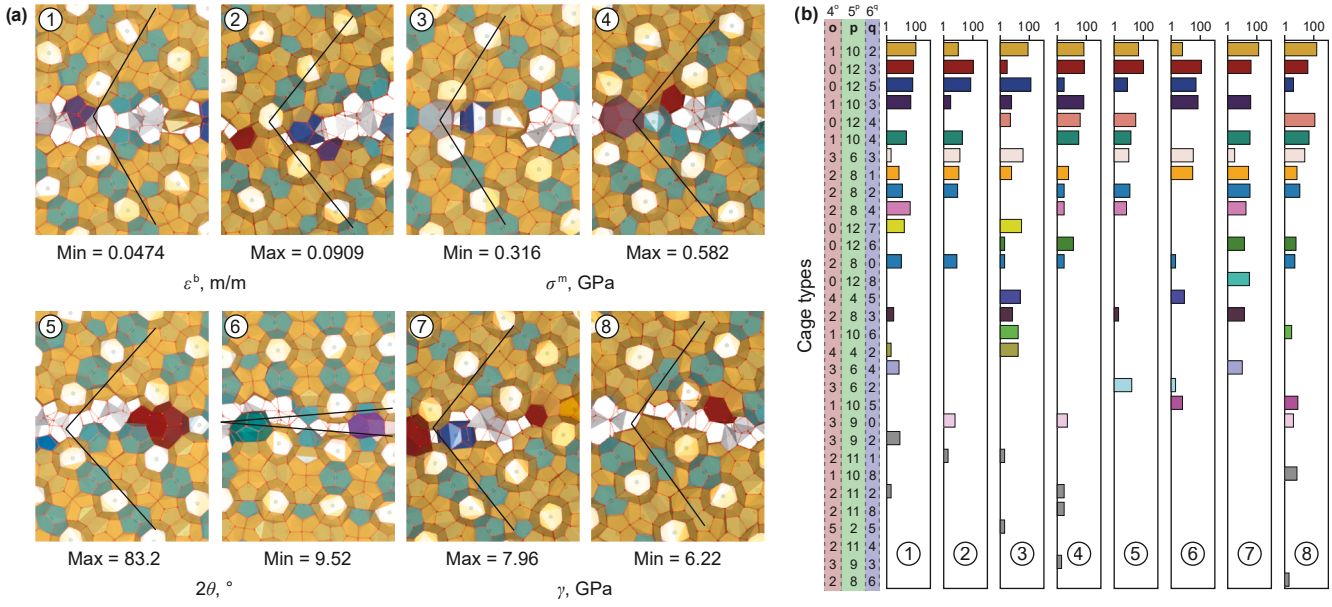

Fig. 2. (**a**) Zoomed-in configurations of GBs in polycrystalline methane hydrates, in which GBs are selected in terms of the magnitude of minimum/maximum ultimate strain ($\varepsilon^{b}_{min}/\varepsilon^{b}_{max}$) minimum/maximum strength ($\sigma^{m}_{min}/\sigma^{m}_{max}$), minimum/maximum misorientation angle ($\theta_{min}/\theta_{max}$) and minimum/maximum GB energy ($\gamma_{min}/\gamma_{max}$). Insets of individual cages indicate the marks of the type of cages, for example, 0–12–2 and 0–12–0 indicate $5^{12}6^{2}$ and 5^{12} cages, respectively. (**b**) The number of 40 types of clathrate cages identified from abovementioned 8 GB samples.

distinct GB microstructures characterized by different clathrate cages and W_A. By comparing the zoomed-in snapshots, bicrystalline methane hydrates with high σ^{m}, large γ and small θ yield richer clathrate cages and low W_A at GBs. This implies that GB of methane hydrate exhibit θ-dependent structural and mechanical properties. Fig. 2(b) shows detail information of 40 types of clathrate cages identified in GBs of bicrystalline methane hydrates with ① ε^{b}_{min} and ② ε^{b}_{max}, ③ σ^{m}_{min} and ④ σ^{m}_{max}, ⑤ θ_{min} and ⑥ θ_{max}, ⑦ γ_{min} and γ_{max}, in which the 40 types of cages are selected based on the largest 40 numbers for all types of cages for all samples. Note that the numbers of cages are time averages during the relaxation process. Apparently, there are pretty diverse cages identified at

GBs, including conventional and unconventional cages. However, there is no clear regularity in the order and number of cages for the GBs of bicrystalline methane hydrates, indicating the complexity of GB structures in methane hydrates. In addition, upon external disturbances, GB microstructures are dynamical changes and thereby are multiple metastable configurations, for example, cages undergo reversible cage conversions because there is minor energy difference between cage structures before and after cage conversions. Figs. S3–S5 shows the diversity in the clathrate cages at GBs with θ varying from 5.19° to 40.6°, as well as the fluctuations in the number of clathrate cages with uniaxial strain for GBs with $\theta = 5.19°$, 14.04° and 36.87°. In a nutshell, GBs of methane hydrates show complex microstructures that are mainly composed of clathrate cages and W_A.

3.2. Descriptors from RF and mechanical properties

As is abovementioned, GBs of methane hydrate show complex solid microstructures, depending on θ. Fig. S6 presents the distribution of W_A, γ, G_L, E, ε^b and σ^m. As is indicated, there are wide distribution in the mechanical properties of GB-contained bicrystalline methane hydrates. This wide range of GB mechanical properties are attributed to the complex GB structures that are dominated by diverse clathrate cages. RF is able to assess the importance of descriptors in the quantitative structure-property relationship (QSPR) model by investigating the deterioration in the model quality when specific descriptors are reduced (Palmer et al., 2007). Furthermore, descriptors with zero weight can be obtained by the RF method. Fig. 3(a)–(d) display the non-zero importance of all cage and global W_A, γ, and θ descriptors, and the prediction of the E of bicrystalline methane hydrate using RF ML model. As is seen, the most significant influences on E of bicrystalline methane hydrates are the global properties of GBs including W_A, γ, and θ, with importance scores of 0.1261, 0.0746, 0.0639, respectively. Using the cage and global W_A, γ, and θ descriptors in the training and predicting E of bicrystalline methane hydrates, the values of root mean square error (RMSE) are determined to around 0.007 and 0.099, respectively. This suggests that as-developed RF ML model shows good performance in predicting the E of bicrystalline methane hydrates. The We now focus on the outcomes using the cage descriptors. Fig. 3(b) shows the weight distribution of the clathrate cages after removing the global descriptors (W_A, γ, and θ), where the orange squares and lines indicate the changes in the weights compared to the case with global

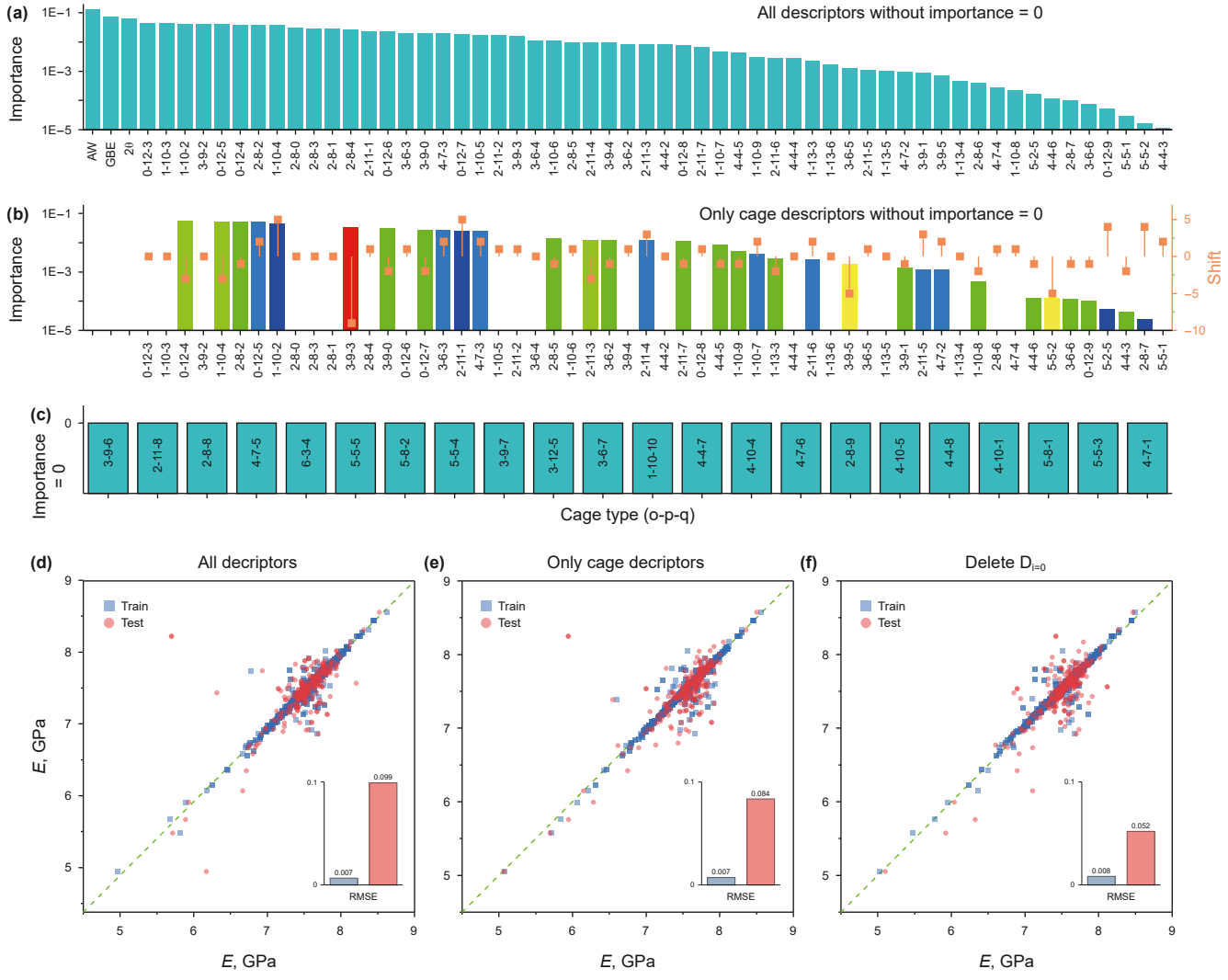

Fig. 3. Prediction of E of bicrystalline methane hydrate by Random Forest (RF) machine learning (ML) models. The importance of input variables including (**a**) all cage and W_A, γ, and θ descriptors, (**b**) all cage descriptors, as well as (**c**) cage descriptors with zero importance evaluated by RF ML models. (**d**)–(**f**) The RF ML predictions of E of bicrystalline methane hydrates using all cage and W_A, γ, and θ descriptors, cage descriptors and only cooperating cage descriptors with non-zero weights against the MD data.

descriptors (W_A, γ, and θ), while Fig. 3(e) displays the corresponding predictions of E against the MD data. Apparently, the weights of different clathrate cages are redistributed when removing the three global descriptors (W_A, γ, and θ). Interestingly, there is no change for the two types of $5^{12}6^3$ and $4^15^{10}6^3$ cages that yield the highest weights among the cage descriptors. This suggests that $5^{12}6^3$ and $4^15^{10}6^3$ cages play critical role in the E of GBs of methane hydrates. In terms of RMSE, they are determined to be 0.007 and 0.084 for the training and testing by a new RF ML model with all cage descriptors, respectively. This indicates that, without the global descriptors (W_A, γ, and θ), as-developed RF ML model with cage descriptors is also able to show good performance in predicting the E of bicrystalline methane hydrates. Fig. 3(c) shows 22 cage types with zero importance in predicting the E of bicrystalline methane hydrate. These types of cages are unconventional cages, with tiny number occurring in finite GBs. Fig. 3(f) presents the prediction of E of bicrystalline methane hydrates using new RF ML model against the MD data, in which the cage descriptors with non-zero importance are utilized. As is observed, as-developed RF model show the RMSE values of 0.008 and 0.052 for the training and testing, respectively, indicting good performance of as-developed RF ML model in the prediction of E of bicrystalline methane hydrate using frequently-occurred cage information.

3.3. Building DNN model

We proceed to train ANN model by excluding the descriptors of cage types with zero weight evaluated by the RF. The details of ANN models are described in Supplementary Material S3.3, as well as the adopted parameters for ANN models. Fig. S7 shows the variation in the RMSE with Epoch step. Apparently, with increasing Epoch step, the reduction in the RMSE becomes less significant, and the RMSE converges within 30,000 Epoch steps. For the specific selection of neural network parameters, please refer to Supplementary Material S3.2.

In neural networks with inappropriate neuron number and structures, two unwanted cases can take place. One is that as neural network is composed of too few neurons or layers, underfit occurs, failing to capture the underlying patterns in the data. In contrast, when neural network consists of too many neurons or layers, overfit appears, causing poor accuracy. Fig. 4 shows the prediction of E of bicrystalline methane hydrates by four ANN models with different neuron numbers and structures. As

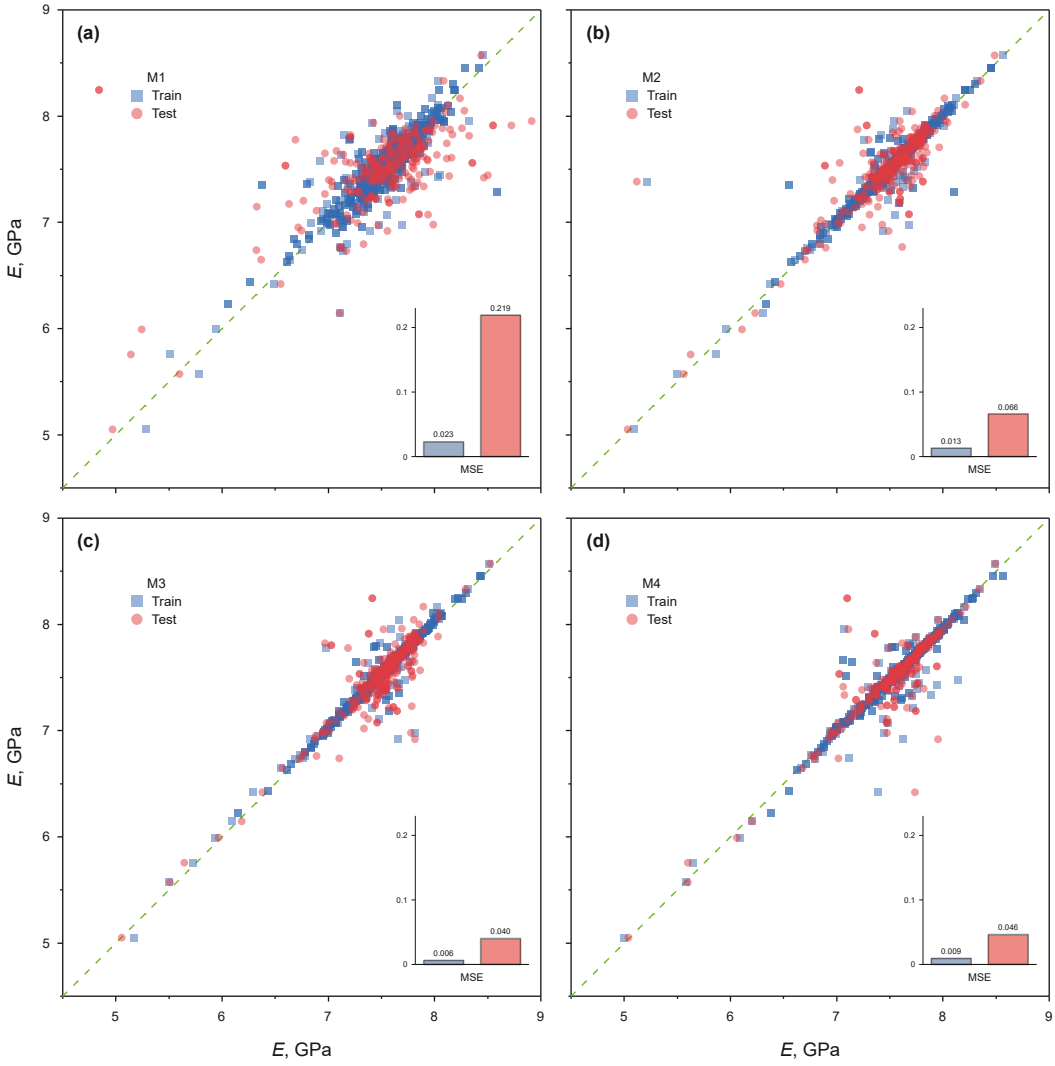

Fig. 4. Prediction of E of bicrystalline methane hydrates results by four ANN models with different neuron compositions. (**a**) One layer with 512 neurons, named as M1. (**b**) Two layers with 512 + 256 neurons, named as M2. (**c**) Three layers with 1024 + 512 + 256 neurons, named as M3. (**d**) Six layers with 1024 + 1024 + 512 + 512 + 256 + 256 neurons, named as M4.

indicated, ANN M1-4 models with different neuron numbers and structures yield distinct accuracy and performance in predicting the E of bicrystalline methane hydrates. With increasing the neuron number from 512 to 1792 and layers from 1 to 3, ANN model yields better performance in predicting E of bicrystalline methane hydrates in terms of RMSE. With further increasing the neuron number and layers to 3584 and 6, however, there is reduction in the performance of ANN model in predicting the E of GB-contained bicrystalline methane hydrates in terms of RMSE. In a nutshell, ANN-M3 model demonstrates the best performance in predicting the E of bicrystalline methane hydrates.

3.4. Prediction of GB mechanical properties

After determining the parameters and the descriptors for ANN model (ANN-M3), we proceed with training ANN-M3 ML model in predicting various mechanical properties of GB-contained bicrystalline methane hydrates (Fig. 5(a)). The uniaxial tensile stress-strain curves of all GB-contained bicrystalline samples are shown in Fig. 5(b), while Fig. 5(c)–(f) displays the variation in the γ, E, ε^{b} and σ^{m} with θ. Apparently, it is difficult to establish intrinsic relationships of structural/mechanical properties and θ. As a result, ANN model is required to establish quantitative structure-mechanical properties relationships. The dataset of GB structures is divided into three parts, with 68% for training, 15% for validation, and 17% for testing. To identify overfitting or selection bias, 10-fold cross-validations to test the accuracy of as-trained ANN-M3 model. All input values are normalized between 0 and 1 to ensure an evenly distributed feature space. The optimized ANN-M3 structure (DNN-M3) is used for model training. Fig. 5(g)–(f) shows the predictive results under the framework of as-developed DNN-M3 ML model, with training errors of $\gamma = 0.0188$ kcal·mol^{-1}·nm^{-2}, $\varepsilon^{b} = 0.00134$, $\sigma^{m} = 0.00985$ GPa, and $E = 0.0708$ GPa, respectively. Such a DNN-based ML framework can well predict the mechanical properties of GBs in methane hydrates. Note that, for all ANN ML models, particularly for the DNN models, the selection of training parameters is time-consuming. Additionally, many efforts should be made to ensure data integrity, ensuring the most significant features are included. A tabular summary (excel sheet source) comparing the microstructural features and mechanical performance metrics of methane hydrates with different GB configurations is insert in the end of the Supplementary Material.

3.5. Reduced descriptors by PCA

Although DNN-M3 ML model yields good performance in predicting the structural and mechanical properties of GBs in methane hydrates, the large number of cage descriptors is utilized as inputs. Principal component analysis (PCA) is widely used in ML

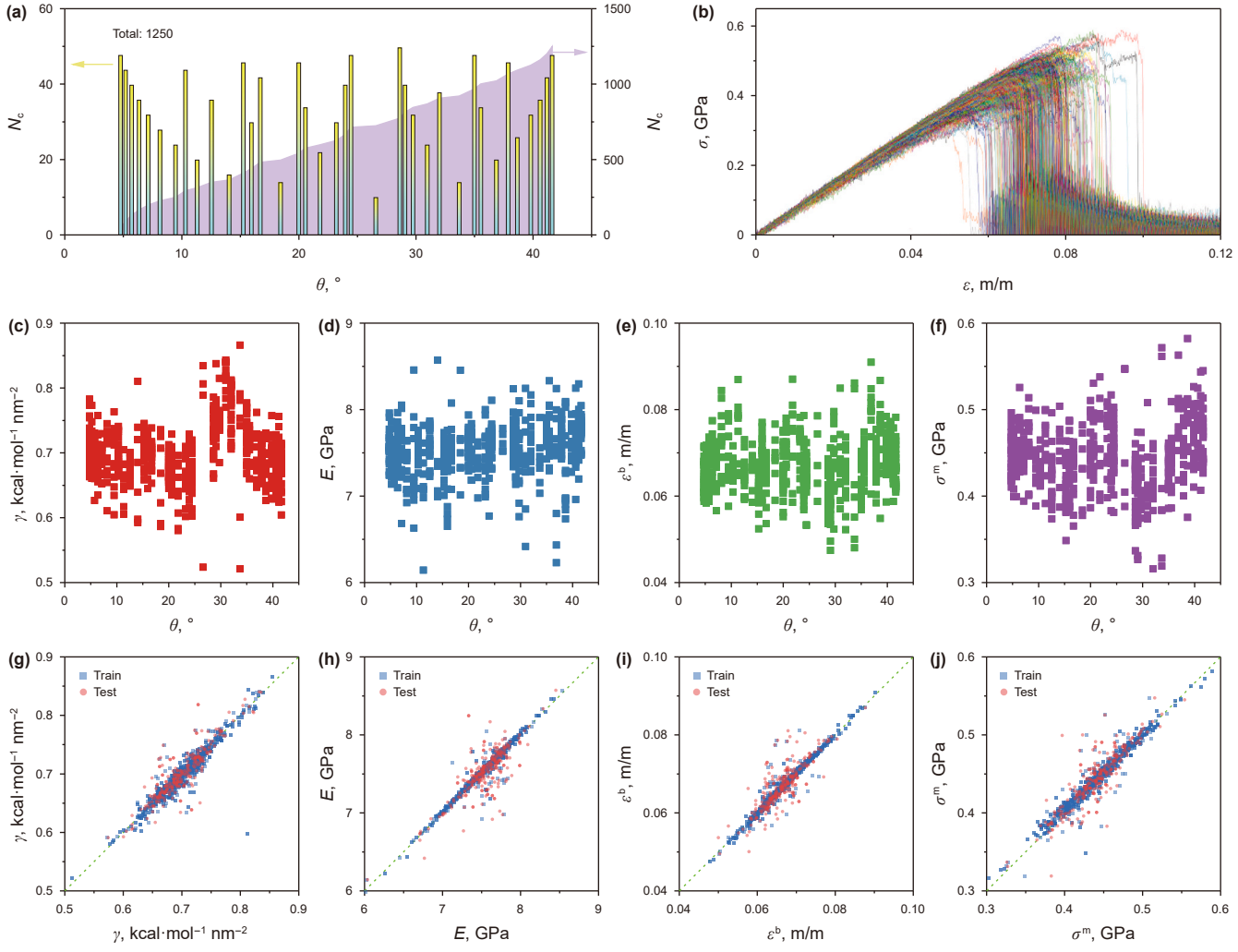

Fig. 5. (**a**) The number of GB models with different misorientation angles (θ), as well as the accumulating number of GB models with increasing θ. (**b**) Uniaxial tensile stress-strain curves of symmetrical GBs in methane hydrates for all training datasets. (**c**)–(**f**) γ, E, ε^{b} and σ^{m} as a function of θ for all GB samples, respectively. (**g**)–(**j**) GB properties of γ, E, ε^{b} and σ^{m} in methane hydrate by DNN-M3 models against the MD data.

algorithms across various disciplines to address multicollinearity and reduce the number of variables used as inputs for ML study (Howley et al., 2006). Here, the PCA is adopted to reduce the number of descriptors and identify the critical cage types influencing the mechanical properties of GBs in methane hydrate. As is illustrated in Fig. 6(a) and (b), the PCA plots change significantly when the non-cage descriptors are removed. It is observed from Fig. 6(b) and (c) that when the cage type descriptors with zero importance obtained from the RF Model are excluded, however, there are insignificant changes in the PCA plots. With further reducing cage types, it is revealed from Fig. 6(c) and (d) that there are minor changes in the PCA plots. As is indicated in Fig. 6(d), 11 types of cages including $5^{12}6^8$, $4^15^{10}6^6$, $5^{12}6^7$, $4^15^{10}6^5$, $5^{12}6^4$, $4^25^86^1$, $4^25^86^2$, $4^15^{10}6^4$, $4^15^{10}6^3$, $5^{12}6^5$ and $5^{12}6^3$ are the most significant cages influencing the prediction of mechanical properties of GBs in methane hydrate. Fig. 6(e) and (f) show the changes in the density of these 11 cages with ε^b for all GB samples. For GB structures with lower ultimate strain ε^b, the number and proportion of these 11

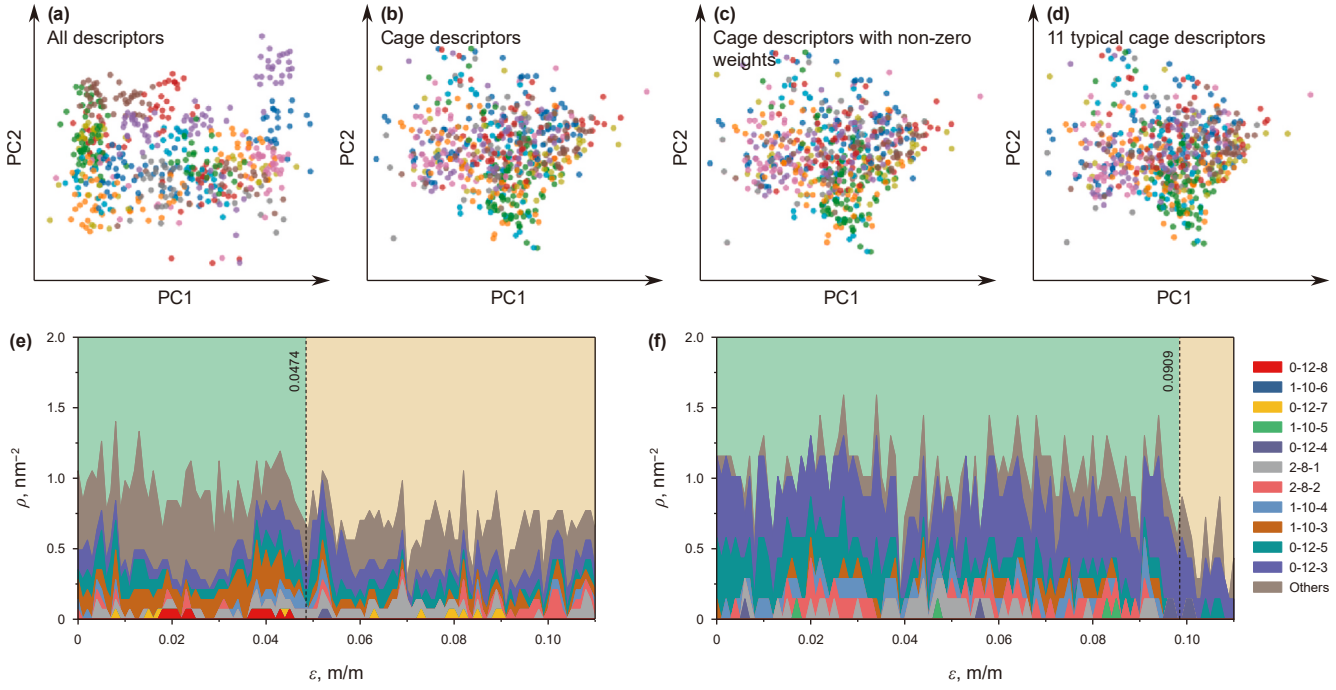

Fig. 6. (**a**)–(**d**) Distributions of PCA features obtained by RF ML models. (**e**) and (**f**) The changes in the number of $5^{12}6^8$, $4^15^{10}6^6$, $5^{12}6^7$, $4^15^{10}6^5$, $5^{12}6^4$, $4^25^86^1$, $4^25^86^2$, $4^15^{10}6^4$, $4^15^{10}6^3$, $5^{12}6^5$ and $5^{12}6^3$ cages in the GB structures with ε.

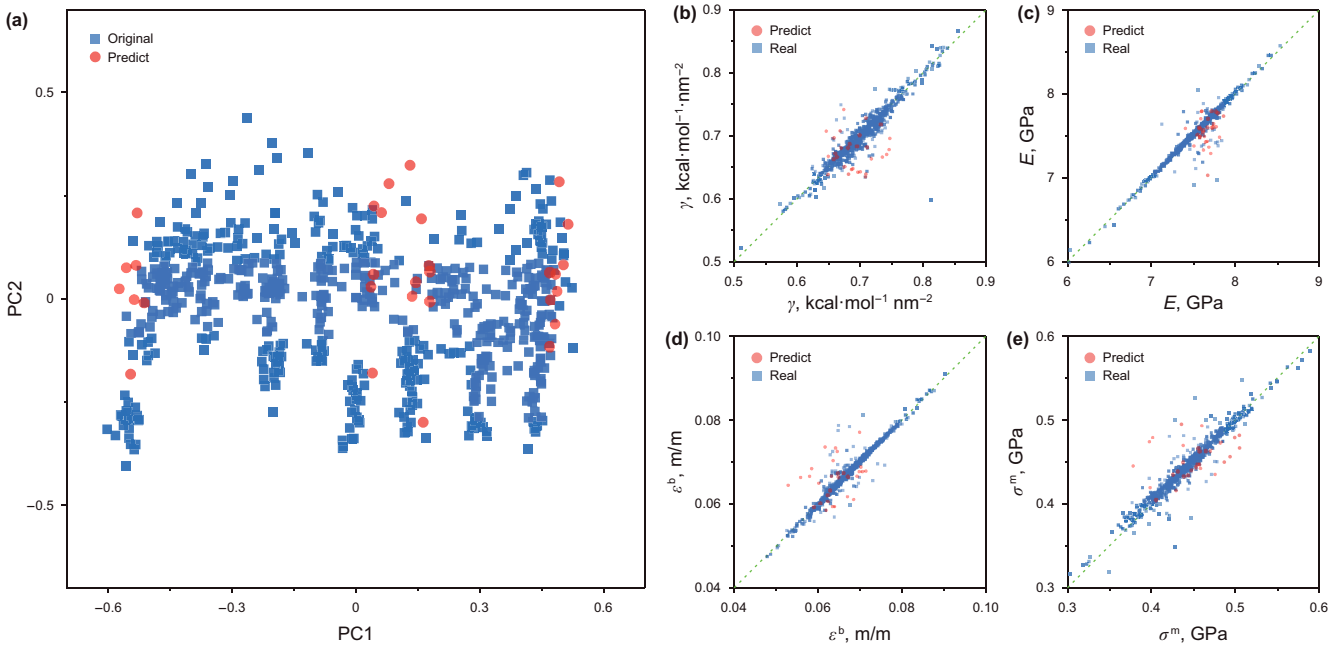

Fig. 7. (**a**) Distribution of PCA features with predicted (red cycle) and original (blue square) values. (**b**)–(**e**) Predictions of γ, E, ε^b and σ^m of GBs in methane hydrates against MD data, respectively.

types of cage are fewer found. In contrast, for GB structures with high ultimate strain ε^{b}, the number and proportion of these 11 types of cage are frequently-observed.

In addition, 30 GBs with large θ are further created to confirm the accuracy of as-developed DNN-M3 ML model. Fig. 7(a) shows the PCA diagram, in which the blue square and red dots represent the original and newly-generated GB models. Fig. 7(b)–(e) show the prediction of γ, E, ε^{b} and σ^{m} of GBs in methane hydrates by as-developed DNN-M3 ML model. As is indicated, as-developed DNN-M3 ML model show good performance in prediction of the mechanical properties of newly-generated GBs, demonstrating the scalability of as-developed DNN ML model. Promising experimental techniques such as q Plus-based low-temperature atomic force microscope (Hong et al., 2024) for achieving reliable measurements of the mechanical properties of polycrystalline methane hydrates are expected to facilitate future validation of the computational predictions presented in this work.

4. Conclusions

In summary, the microstructures and mechanical properties of GBs of methane hydrates with wide range of θ generated by the CSL model are examined using MD simulations. The GB structures are characterized by 84 features including G_L, γ, θ, W_A and 80 types of cage types that are selected as descriptors for ML study. Descriptors with zero importance are then screened using RF method. Based on the structural characteristics, DNN ML models with four different neuron numbers and structures are developed to predict the structural and mechanical properties of GBs of methane hydrate including γ, E, ε^{b} and σ^{m}. Furthermore, PCA method is adopted to refine the descriptors, reducing the descriptors down to 11 types of cages to well predict the mechanical properties of GBs of methane hydrates. Our as-developed DNN-based ML model demonstrates high-accuracy in predicting GB properties of methane hydrates, which is of critical importance in the understanding of mechanical stability of sediment-hosted NGHs.

CRediT authorship contribution statement

Ke Xu: Software, Investigation, Data curation, Writing – original draft, Methodology, Formal analysis. **Rui Ma:** Software, Formal analysis, Writing – review & editing, Methodology. **Yong-Xiao Qu:** Software, Formal analysis, Writing – review & editing, Methodology. **Zhi-Sen Zhang:** Writing – review & editing, Resources, Formal analysis, Visualization, Methodology. **Jian-Bin Xu:** Supervision, Funding acquisition, Writing – review & editing, Project administration, Formal analysis. **Jian-Yang Wu:** Writing – review & editing, Resources, Funding acquisition, Conceptualization, Supervision, Project administration, Formal analysis.

Declaration of competing interest

The authors declare that they have no known competing financial interests or personal relationships that could have appeared to influence the work reported in this paper.

Acknowledgments

This work is financially supported by the National Natural Science Foundation of China (Grant Nos. 12172314, 12572127, 11772278, and 11904300), the Jiangxi Provincial Outstanding Young Talents Program (Grant No. 20192BCBL23029), and the 111 Project (B16029). The supercomputer GPU hours are provided by Shao-Rong Fang and Tian-Fu Wu from Information and Network Center of Xiamen University, and they are acknowledged for the help with the high-performance computer.

Appendix A. Supplementary data

Supplementary data to this article can be found online at https://doi.org/10.1016/j.petsci.2025.10.018.

References

Boswell, R., 2009. Is gas hydrate energy within reach? Science 325, 957–958. https://doi.org/10.1126/science.1175074.
Cao, P.Q., Sheng, J.L., Wu, J.Y., Ning, F.L., 2021. Mechanical creep instability of nanocrystalline methane hydrates. Phys. Chem. Chem. Phys. 23 (5), 3615–3626. https://doi.org/10.1039/D0CP05896C.
Durham, W.B., Stern, L.A., Kirby, S.H., 2003a. Ductile flow of methane hydrate. Can. J. Phys. 81, 373–380. https://doi.org/10.1139/p03-042.
Durham, W.B., Kirby, S.H., Stern, L.A., Zhang, W., 2003b. The strength and rheology of methane clathrate hydrate. J. Geophys. Res. Solid Earth 108 (B4), 2182. https://doi.org/10.1029/2002JB001872.
Freij-Ayoub, R., Tan, C., Clennell, B., Tohidi, B., Yang, J.H., 2007. A wellbore stability model for hydrate bearing sediments. J. Petrol. Sci. Eng. 57, 209–220. https://doi.org/10.1016/j.petrol.2005.10.011.
Hester, K.C., Brewer, P.G., 2009. Clathrate hydrates in nature. Ann. Rev. Mar. Sci 1, 303–327. https://doi.org/10.1146/annurev.marine.010908.163824.
Hong, J.N., Tian, Y., Liang, T.C., Liu, X.M., Song, Y.Z., Guan, D., Yan, Z.X., Guo, J.D., Tang, B.Z., Cao, D.Y., Guo, J., Chen, J., Pan, D., Xu, L.M., Wang, E.G., Jiang, Y., 2024. Imaging surface structure and premelting of ice Ih with atomic resolution. Nature 630, 375–380. https://doi.org/10.1038/s41586-024-07427-8.
Howley, T., Madden, M.G., O'Connell, M.L., Ryder, A.G., 2006. The effect of principal component analysis on machine learning accuracy with high-dimensional spectral data. Knowl. Base Syst. 19 (5), 363–370. https://doi.org/10.1016/j.knosys.2005.11.014.
Kvenvolden, K.A., 1999. Potential effects of gas hydrate on human welfare. Proc. Natl. Acad. Sci. 96 (7), 3420–3426. https://doi.org/10.1073/pnas.96.7.3420.
Li, X.S., Xu, C.G., Zhang, Y., Ruan, X.K., Li, G., Wang, Y., 2016. Investigation into gas production from natural gas hydrate: A review. Appl. Energy 172, 286–322. https://doi.org/10.1016/j.apenergy.2016.03.101.
Liu, H., Li, H.S., Yao, D.S., Guo, P., Wen, L.H., 2022a. The research on the natural gas hydrate dissociation kinetic from hydrate-sediments/seawater slurries. Chem. Eng. J. 435, 135127. https://doi.org/10.1016/j.cej.2022.135127.
Liu, L.P., Ryu, B., Sun, Z.L., Wu, N.Y., Cao, H., Geng, W., Zhang, X.R., Jia, Y.G., Xu, C.L., Guo, L., Wang, L.B., 2019. Monitoring and research on environmental impacts related to marine natural gas hydrates: Review and future perspective. J. Nat. Gas Sci. Eng. 65, 82–107. https://doi.org/10.1016/j.jngse.2019.02.007.
Liu, Y.S., Xu, K., Xu, Y.H., Liu, J.J., Wu, J.Y., Zhang, Z.S., 2022b. HTR: An ultra-high speed algorithm for cage recognition of clathrate hydrates. Nanotechnol. Rev. 11, 699–711. https://doi.org/10.1515/ntrev-2022-0044.
Lu, Y.Y., Ge, B.B., Zhong, D.L., 2020. Investigation of using graphite nanofluids to promote methane hydrate formation: Application to solidified natural gas storage. Energy 199, 117424. https://doi.org/10.1016/j.energy.2020.117424.
Max, M.D., Johnson, A.H., Dillon, W.P., Osegovic, J.P., Tatro, S.R., Holman, S.A., 2006. Physical chemical characteristics of natural gas hydrate. Econ. Geol. Nat. Gas Hydr. 45–104. https://doi.org/10.1007/1-4020-3972-7_3.
Murshed, M.M., Klapp, S.A., Enzmann, F., Szeder, T., Huthwelker, T., Stampanoni, M., Marone, F., Hintermüller, C., Bohrmann, G., Kuhs, W.F., Kersten, M., 2008. Natural gas hydrate investigations by synchrotron radiation X-ray cryo-tomographic microscopy (SRXCTM). Geophys. Res. Lett. 35. https://doi.org/10.1029/2008GL035460.
Ning, F.L., Yu, Y.B., Kjelstrup, S., Vlugt, T.J.H., Glavatskiy, K., 2012. Mechanical properties of clathrate hydrates: status and perspectives. Energy Environ. Sci. 5, 6779–6795. https://doi.org/10.1039/C2EE03435B.
Ota, M., Morohashi, K., Abe, Y., Watanabe, M., Smith, J.R.L., Inomata, H., 2005. Replacement of CH_4 in the hydrate by use of liquid CO_2. Energy Convers. Manag. 46, 1680–1691. https://doi.org/10.1016/j.enconman.2004.10.002.
Palmer, D.S., O'Boyle, N.M., Glen, R.C., Mitchell, J.B.O., 2007. Random forest models to predict aqueous solubility. J. Chem. Inf. Model. 47, 150–158. https://doi.org/10.1021/ci060164k.
Pang, X.Q., Chen, Z.H., Jia, C.Z., Wang, E.Z., Shi, H.S., Wu, Z.Y., Hu, T., Liu, K.Y., Zhao, Z.F., Pang, B., Wang, T., 2021. Evaluation and re-understanding of the global natural gas hydrate resources. Pet. Sci. 18, 323–338. https://doi.org/10.1007/s12182-021-00568-9.
Peters, B., Zimmermann, N.E.R., Beckham, G.T., Tester, J.W., Trout, B.L., 2008. Path sampling calculation of methane diffusivity in natural gas hydrates from a water-vacancy assisted mechanism. J. Am. Chem. Soc. 130, 17342–17350. https://doi.org/10.1021/ja802014m.
Qin, Y., Pan, Z., Liu, Z.M., Shang, L.Y., Zhou, L., 2021. Influence of the particle size of porous media on the formation of natural gas hydrate: A review. Energy Fuel. 35, 11640–11664. https://doi.org/10.1021/acs.energyfuels.1c00936.
Sloan, E.D., 2003. Fundamental principles and applications of natural gas hydrates. Nature 426, 353–359. https://doi.org/10.1038/nature02135.

Stern, L.A., Kirby, S.H., Durham, W.B., 1996. Peculiarities of methane clathrate hydrate formation and solid-state deformation, including possible superheating of water ice. Science 273, 1843–1848. https://doi.org/10.1126/science.273.5283.1843.

Stern, L.A., Kirby, S.H., Durham, W.B., 1998. Polycrystalline methane hydrate: synthesis from superheated ice, and low-temperature mechanical properties. Energy Fuel. 12, 201–211. https://doi.org/10.1021/ef970167m.

Sveinsson, H.A., Ning, F.L., Cao, P.Q., Fang, B., Malthe-Sørenssen, A., 2021. Grain-size-governed shear failure mechanism of polycrystalline methane hydrates. J. Phys. Chem. C 125, 10034–10042. https://doi.org/10.1021/acs.jpcc.1c00901.

Tung, Y.T., Chen, L.J., Chen, Y.P., Lin, S.T., 2011. In situ methane recovery and carbon dioxide sequestration in methane hydrates: A molecular dynamics simulation study. J. Phys. Chem. B 115, 15295–15302. https://doi.org/10.1021/jp2088675.

Vlasic, T.M., Servio, P.D., Rey, A.D., 2017. Effect of guest size on the mechanical properties and molecular structure of gas hydrates from first-principles. Cryst. Growth Des. 17, 6407–6416. https://doi.org/10.1021/acs.cgd.7b01072.

Wei, N., Pei, J., Li, H.T., Zhou, S.W., Zhao, J.Z., Kvamme, B., Coffin, R.B., Zhang, L.H., Zhang, Y., Xue, J., 2024. Classification of natural gas hydrate resources: Review, application and prospect. Gas Sci. Eng. 124, 205269. https://doi.org/10.1016/j.jgsce.2024.205269.

Wu, J.Y., Ning, F.L., Trinh, T.T., Kjelstrup, S., Vlugt, T.J.H., He, J.Y., Skallerud, B.H., Zhang, Z.L., 2015. Mechanical instability of monocrystalline and polycrystalline methane hydrates. Nat. Commun. 6, 8743. https://doi.org/10.1038/ncomms9743.

Yu, C.H., Chen, L.T., Sun, B.J., 2019. Experimental characterization of guest molecular occupancy in clathrate hydrate cages: A review. Chin. J. Chem. Eng. 27, 2189–2206. https://doi.org/10.1016/j.cjche.2019.03.026.

Zhang, M., Niu, M., Shen, S.W., Dai, S.L., Xu, Y., 2021a. Review of natural gas hydrate dissociation effects on seabed stability. Nat. Hazards 107, 1035–1045. https://doi.org/10.1007/s11069-021-04629-5.

Zhang, X.M., Zhang, S.L., Yin, S.Q., He, G.Y., Li, J.P., Wu, Q.B., 2022. Research progress of the kinetics on natural gas hydrate replacement by CO_2-containing mixed gas: A review. J. Nat. Gas Sci. Eng. 108, 104837. https://doi.org/10.1016/j.jngse.2022.104837.

Zhang, Y.L., Taboada-Serrano, P., 2020. Model for gas-hydrate equilibrium in porous media that incorporates pore-wall properties. Phys. Chem. Chem. Phys. 22, 10900–10910. https://doi.org/10.1039/D0CP01263G.

Zhang, Z.C., Kusalik, P.G., Guo, G.J., Ning, F.L., Wu, N.Y., 2021b. Insight on the stability of polycrystalline natural gas hydrates by molecular dynamics simulations. Fuel 289, 119946. https://doi.org/10.1016/j.fuel.2020.119946.

Zi, M.C., Chen, D.Y., Wu, G.Z., 2018. Molecular dynamics simulation of methane hydrate formation on metal surface with oil. Chem. Eng. Sci. 191, 253–261. https://doi.org/10.1016/j.ces.2018.06.070.